BeBeC-2026-S06

APPLICATION OF UNFOLDED SHRINKAGE-THRESHOLDING ALGORITHMS FOR THE ANALYSIS OF AEROACOUSTIC MEASUREMENTS

Adam Kujawski and Ennes Sarradj
TU Berlin, FG Technische Akustik
Einsteinufer 25, 10587 Berlin, Germany

Abstract

Many inverse and deconvolution methods in microphone array processing can be formulated as least-squares problems for estimating spatial sound source distributions. In particular, regularized formulations, such as Lasso, are widely used to promote sparsity and to improve robustness against measurement noise and model mismatch. Traditionally, these problems are solved with model-based optimization algorithms that require model selection to determine the regularization parameter value. More recently, data-driven alternatives have been proposed that unfold the iterations of model-based algorithms and learn relevant parameters from data. Such approaches can substantially reduce computational cost at inference time. Usually, unfolded algorithms are trained in a supervised manner, which would require ground-truth source maps that are generally unavailable for experimental aeroacoustic measurements. A possible alternative is to train the unfolded algorithm by minimizing the underlying optimization objective, using regularization parameters from previous model selections with model-based solvers. In this work, an unfolded variant of the Fast Iterative Shrinkage-Thresholding Algorithm (FISTA) as part of the Covariance Matrix Fitting (CMF) method is trained in an unsupervised manner based on microphone array signals of a NACA 63-018 airfoil model measured in an open-jet wind tunnel. After training, the unfolded CMF algorithm produces source maps comparable to those obtained with model-based FISTA, while using 200 times fewer iterations and reducing the average processing time from 8.64 s to 0.33 s per measurement.

1 INTRODUCTION

Acoustic testing with microphone arrays often involves measurement campaigns in which array methods are applied repeatedly to many operating points and configurations. Fast and reliable evaluation methods are therefore required to keep the processing effort manageable. Source characterization is traditionally performed with grid-based frequency-domain methods that reconstruct contributions from individual sources on a predefined focus grid [25]. Classical beamforming and some deconvolution methods are computationally attractive, but their spatial resolution is fundamentally limited by the Rayleigh criterion, leading to inaccurate source strength estimates at low frequencies and for closely spaced sources [31, 37]. Although high-resolution variants exist, their improved reconstruction performance typically comes at substantially higher computational expense [38]. Inverse methods, such as CMF [45, 46], directly fit parameterized source models to measured data and can achieve favorable reconstruction accuracy, particularly at low frequencies and for closely spaced sources, albeit at increased computational cost [17]. Many inverse and deconvolution methods can be formulated as least-squares problems. However, due to the ill-posed nature of the underlying inverse problem, as well as measurement noise and model mismatch, regularization is typically required to obtain meaningful solutions. Classical model selection methods for finding suitable regularization parameters, such as cross-validation or grid search with information criteria, for example the Bayesian Information Criterion (BIC), are computationally expensive. Accordingly, the development of efficient optimization strategies remains an active area of research [10].

As an alternative to model-based optimization, data-driven approaches have recently attracted increasing attention. In particular, various deep learning methods have been applied to acoustic source mapping, although their ability to generalize to unseen measurement conditions and their robustness to model mismatch have yet to be fully established. Emerging from the field of optimization learning [8], unfolded optimization algorithms have been proposed as a data-driven alternative to conventional iterative solvers for inverse problems [26]. These include unfolded variants of the Iterative Shrinkage-Thresholding Algorithm (ISTA) [1, 5, 16, 18, 20, 29, 43], Sparse Bayesian Learning (SBL) [3], Orthogonal Matching Pursuit (OMP) [28], and Non-Negative Least Squares (NNLS) [35]. In microphone array processing, unfolded proximal-gradient methods in particular have shown promising performance as optimization strategies [7, 19, 21, 30] for the CMF method and the Deconvolution Approach for the Mapping of Acoustic Sources (DAMAS), not only in terms of computational efficiency but also with respect to reconstruction accuracy. However, improved reconstruction accuracy is typically achieved through supervised training, which enables the network to learn the desired reconstruction directly rather than the solution of the underlying optimization problem. As a result, ground-truth source maps are required for training, but such references are generally unavailable in complex experimental scenarios such as aeroacoustic measurements.

This work investigates whether unfolded algorithms for the CMF problem can be effectively trained using only experimental data from aeroacoustic measurements without providing explicit ground-truth source maps. The aim is to assess whether such a trained solver can provide a computationally efficient alternative to model-based algorithms. For this purpose, an unfolded variant of FISTA is trained directly on measured microphone-array data from different airfoil configurations by minimizing the Lasso objective, using regularization parameters obtained from previous model-based FISTA evaluations. The results show that, once the training is complete, the unfolded algorithm produces source maps comparable to model-based FISTA with

substantially fewer iterations and without repeated model selection during reconstruction.

2 PRELIMINARIES

2.1 Covariance Matrix Fitting

Using Welch's method [41], the measured Cross-Spectral Matrix (CSM) of the microphone signals for an array with c channels at a given frequency is estimated from B snapshots as

$$C = \frac{1}{B}\sum_{b=1}^{B} p_b p_b^{\mathsf{H}} \in \mathbb{C}^{c\times c}, \tag{1}$$

where $p_b \in \mathbb{C}^c$ holds the sound pressure values of all microphones for the bth snapshot. In aeroacoustic wind-tunnel measurements, the diagonal entries of the CSM are particularly affected by noise [13, 36]. Therefore, removing the diagonal is a standard approach to suppress this noise, which is valid under the assumption that the noise is uncorrelated between spatially separated microphones so that it does not contaminate the off-diagonal entries. More advanced denoising methods have been proposed in the literature [12].

The *CMF* method [45] aims to minimize the discrepancy between the measured CSM and a modeled one by reconstructing the source distribution on a predefined focus grid. Assuming a linear propagation model, the noise-free CSM can be modeled as

$$C_{\mathrm{mod}} = HQ_sH^{\mathsf{H}}, \tag{2}$$

where $H \in \mathbb{C}^{c\times n}$ is the transfer matrix and $Q_s \in \mathbb{C}^{n\times n}$ is the source CSM. In Eq. (2), the microphone signals are related to the source signals through the transfer matrix

$$H_{i,j} = \frac{r_{0,j}}{r_{i,j}} \exp\left(-\mathrm{i}2\pi f\left(t_{i,j} - t_{0,j}\right)\right), \tag{3}$$

where $i \in \{1,\dots,c\}$ and $j \in \{1,\dots,n\}$ denote the microphone and focus-point indices, respectively. Here, $t_{i,j}$ and $r_{i,j}$ denote the travel time and distance from source point j to microphone i, while $t_{0,j}$ and $r_{0,j}$ are the corresponding quantities for the reference location. Furthermore, f is the frequency, $\mathrm{i} = \sqrt{-1}$ the imaginary unit, and n the number of grid points in the source region. In this work, the travel times are obtained by a fast ray-casting method that accounts for sound refraction at the shear layer [33].

Under the assumption of mutually uncorrelated sources, $Q_s = \mathrm{diag}(x)$ with source strengths $x \in \mathbb{R}^n_+$. In addition, only the strictly upper-triangular entries of the CSM carry unique information, since the CSM is Hermitian and the diagonal entries are discarded. Vectorization of Eq. (2), using only the upper-triangular entries and casting the problem in real-valued form, yields a linear model of the form $Ax = y_{\mathrm{mod}}$, where $A \in \mathbb{R}^{m\times n}$ is the sensing matrix with $m = c(c-1)$ and $y_{\mathrm{mod}} = \mathrm{vec}(C_{\mathrm{mod}}) \in \mathbb{R}^m$.

In practice, the measured CSM C is subject to estimation errors from the finite number of snapshots. In addition, the assumed source propagation and radiation model required to define A is only an approximation and model mismatch is inevitable. Therefore, the linear model does not hold exactly, and an infinite number of solutions exist. To account for the ill-posed nature of

the inverse problem and to promote a sparse solution, an ℓ_1 penalty is commonly added, leading to the positivity-constrained and regularized least-squares problem

$$\hat{x} = \arg\min_{x \geq 0} \left\{ \frac{1}{2} \|Ax - y\|_2^2 + \lambda \|x\|_1 \right\}, \tag{4}$$

where $\lambda > 0$ controls the sparsity of the solution.

The process of finding a suitable regularization parameter λ is known as *model selection*, which is crucial for obtaining meaningful source mappings. Common approaches include k-fold cross-validation, which selects λ by minimizing prediction error on held-out data, and information-criterion-based methods such as the BIC and its extensions [42]. In this work, grid search with the BIC is used to select λ for the model-based optimization methods.

2.2 Iterative Thresholding Algorithms

A standard iterative solver for the regularized least-squares problem is the ISTA [4], which alternates between a gradient step on the least-squares term and the application of the soft-thresholding operator enforcing the regularization constraint. With step size $\gamma = 1/L$, where $L = \eta_{\max}(A^\top A)$ and $\eta_{\max}$ corresponds to the largest eigenvalue of $A^\top A$, one iteration reads

$$x^{(k+1)} = S_\theta \left(x^{(k)} + \gamma A^\top \left(y - A x^{(k)} \right) \right), \tag{5}$$

where the soft-thresholding operator $S_\theta(z) = \operatorname{sign}(z)(|z| - \theta)_+$ is applied element-wise, with threshold $\theta = \lambda\gamma$, and initialized with $x^{(0)} = 0$. To accelerate convergence, the FISTA [4] applies the gradient step to a momentum-extrapolated iterate $z^{(k)}$ rather than $x^{(k)}$:

$$t_{k+1} = \frac{1 + \sqrt{1 + 4t_k^2}}{2}, \tag{6}$$

$$z^{(k)} = x^{(k)} + \frac{t_k - 1}{t_{k+1}} \left(x^{(k)} - x^{(k-1)} \right), \tag{7}$$

$$x^{(k+1)} = S_\theta \left(z^{(k)} + \gamma A^\top \left(y - A z^{(k)} \right) \right), \tag{8}$$

with $t_1 = 1$ and $x^{(0)} = z^{(0)} = 0$. A positivity-constrained variant of ISTA and FISTA has been derived in [48], for which the standard soft-thresholding operator is replaced by $S_\theta^+(z) = (|z| - \theta)_+$.

3 MICROPHONE ARRAY DATA

3.1 Measurement Campaign

The microphone array data used in the present work stem from a measurement campaign conducted in the acoustic wind tunnel of TU Berlin, an open-jet facility with a rectangular nozzle exit section of $0.40\,\mathrm{m} \times 0.33\,\mathrm{m}$. The jet discharged into an anechoic chamber of volume $V = 830\,\mathrm{m}^3$ with a lower cut-off frequency of 63 Hz. Figure 1 shows the measurement setup.

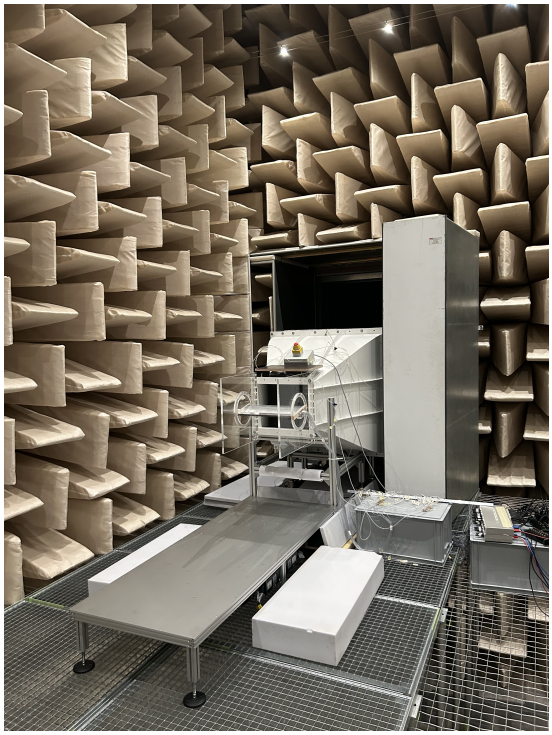

(a) Open-jet test section in the anechoic chamber with the planar microphone array below the airfoil model.

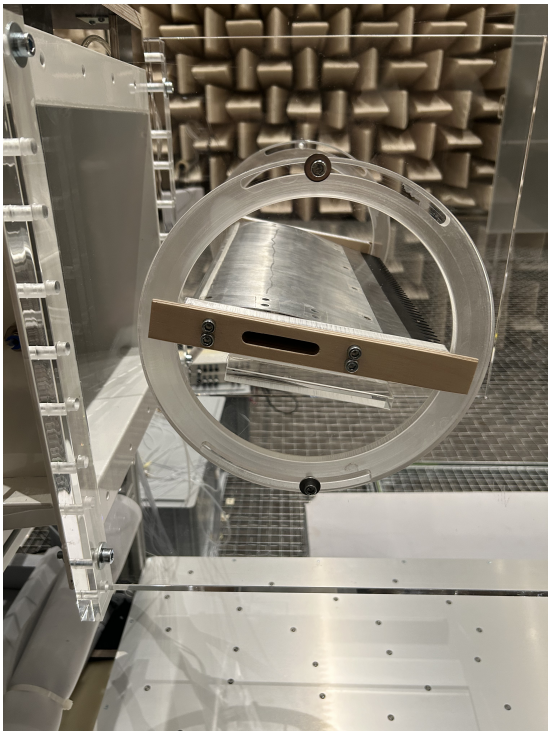

(b) Sideview of the NACA 63-018 airfoil model with serrations mounted between circular side-plate inserts.

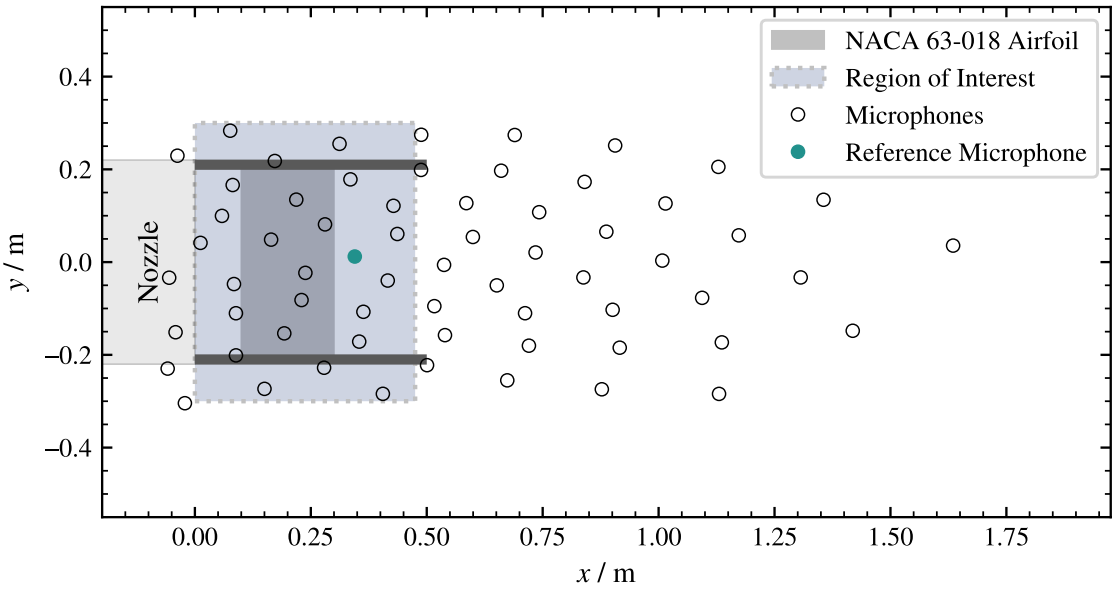

(c) Schematic of the measurement setup with nozzle exit, airfoil position, discretization area, microphone positions, and reference microphone position. (view from below the airfoil model)

Figure 1: Microphone array measurement setup for the NACA 63-018 airfoil.

The model under test was a NACA 63-018 airfoil (see [14] for details) with a chord length of 0.2 m, a span of 0.4 m, and a trailing-edge thickness of 0.3 mm. It was mounted by circular inserts between two rectangular side plates of size 0.5 m × 0.5 m, which were flush with the nozzle lips. The microphone array signals were acquired with a planar array of $c = 64$ GRAS 40PL-1 Short CCP microphones positioned 75 cm below the airfoil. The microphone positions followed a Vogel spiral arrangement [40] with parameters $H_V = 1.0$ and $V_V = 5.0$ according to [32]; the spanwise coordinates were scaled by a factor of 0.4 to fit the nozzle width. Each measurement lasted 40 s and was sampled at 25.6 kHz. The airfoil was measured under the operating conditions summarized in Table 1.

3.2 Microphone Array Data Processing

The microphone array data were processed with the openly available Acoular software [34]. For the present analysis, the 56 microphones closest to the airfoil were used, and the microphone nearest to the trailing edge was used as the reference microphone. The CSM was estimated with Welch's method according to Eq. (1), using a block size of 128 samples, 50 % overlap, and a Hanning window; its diagonal entries were removed. The source region was discretized by a rectangular focus grid covering the airfoil region shown in Fig. 1, with an equidistant spacing of 0.012 m, resulting in $n = 2{,}091$ grid points. Source maps were obtained with the CMF method and FISTA introduced in Sec. 2, using $K = 10{,}000$ iterations. The regularization parameter was selected by grid search based on the BIC. The grid comprised 40 geometrically spaced values starting from the upper limit $\lambda_{\max} = \|A^\top y\|_\infty$, which is the smallest regularization parameter for which the solution satisfies $\hat{x} = 0$ [39]. The ratio between the largest and smallest parameter values was 10^4. In total, 422 measurements were processed for each analyzed frequency. The present work focuses on two representative frequencies, 4 kHz and 8 kHz. Examples of the source maps obtained with FISTA for different flow speeds at 8 kHz and a geometric angle of attack of 0.8° are shown in Fig. 2. Figure 3 shows the corresponding regularization paths for the results given in Fig. 2 and the selected regularization values for all measurements in the dataset at 8 kHz, plotted against the trace of C.

Table 1: Summary of the measured NACA 63-018 airfoil configurations.

Parameter	Summary
Airfoil	small NACA 63-018
Tripping	untripped; tripped (zigzag tape on pressure and suction side)
Serrations	baseline (no serration); straight sawtooth (flap angle 0°); iron-shaped (flap angle 0°); sawtooth (flap angle 4°) upward-mounted; sawtooth downward-mounted
Geom. Angle of Attack	−12° to 24°
Flow speed	5 to 70 m s^{-1}
Acquisition time	$T = 40$ s
Sampling frequency	$f_s = 25.6$ kHz
Temperature	19.7°C to 25.0°C

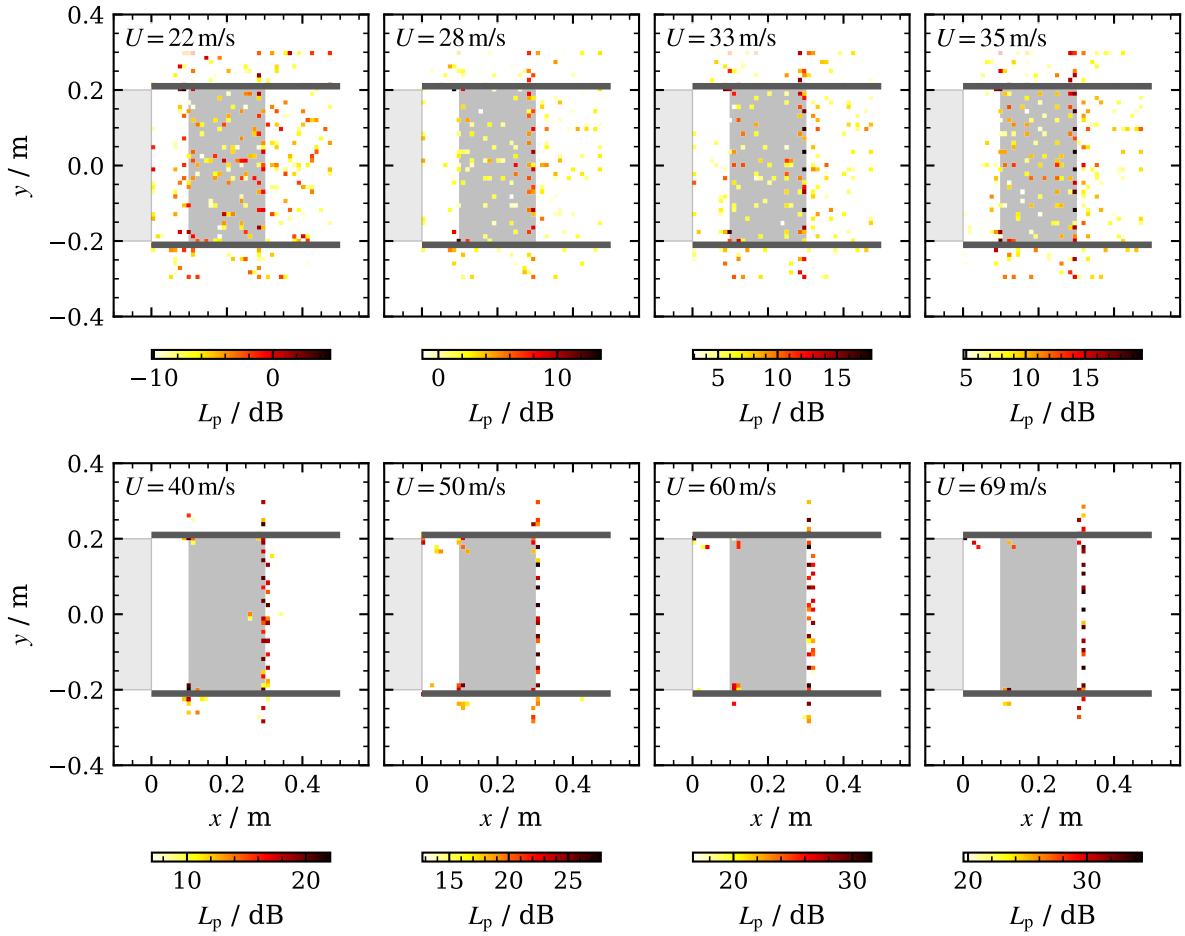

Figure 2: Source map reconstructions at a frequency of 8 kHz *with the* CMF *method and* FISTA *(*$K = 10{,}000$*) based on measurements of the tripped baseline airfoil measured at different flow speeds and a geometric angle of attack of* 0.8°.

4 METHODOLOGY

Source reconstruction using the CMF method, as described above, requires model selection and optimization for every measurement. This is computationally expensive and motivates the search for an optimization strategy that can be learned once from data and then reused for future measurements. Algorithm unfolding provides a suitable framework for this purpose [26]. In this approach, a fixed number of iterations of a model-based solver is interpreted as a neural network architecture, in which selected parts of the optimization algorithm are parameterized and learned from data. Wind-tunnel campaigns for testing airfoil models typically produce numerous microphone array measurements acquired with the same array geometry under different operating conditions, making them well suited for training. For the Lasso problem, numerous unfolded variants of ISTA and FISTA have been proposed [1, 5, 9, 10, 15, 16, 18, 20, 22–24, 29, 44, 47]. However, a direct transfer of these methods to inverse microphone array processing is not straightforward. Much of the literature assumes a single fully known sensing

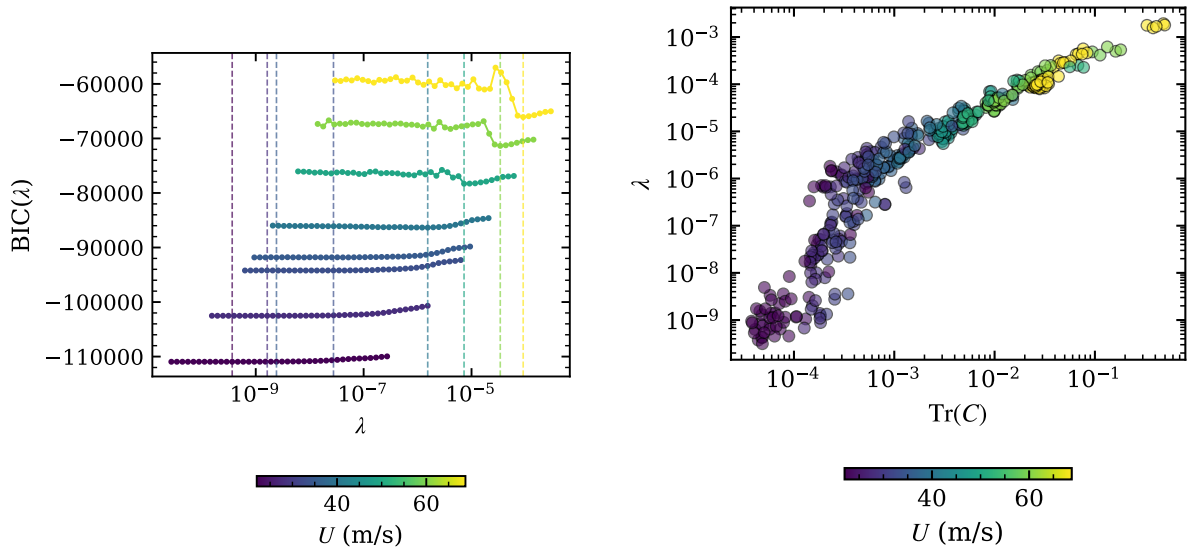

(a) Regularization path for FISTA and the source map reconstructions in Fig. 2. Optimal regularization parameters are indicated by the vertical dashed line.

(b) Selected regularization parameters based on the BIC for all measurements of the dataset at a frequency of 8 kHz over the trace of C.

Figure 3: Optimal regularization parameters based on the BIC at a frequency of 8 kHz.

matrix. In the present application, each measurement d gives rise to a different inverse problem

$$y^{(d)} \approx A^{(d)} x^{(d)}, \qquad d = 1, \ldots, D, \tag{9}$$

because the sensing matrix depends on the measurement conditions, for example the flow speed and temperature. Moreover, the exact propagation model is unavailable in practice, so the reconstruction relies on the approximation $A^{(d)} = A_\star^{(d)} + E^{(d)}$, where $A_\star^{(d)}$ denotes the unknown exact sensing matrix and $E^{(d)}$ summarizes modeling errors. In addition, unfolded algorithms for regularized problems are usually trained in a supervised manner, so that the regularization strength is learned implicitly. Such supervised training requires ground-truth source maps, which are not available for experimental microphone array measurements. One possible solution is to train on simulated data, but this requires the learned algorithm to generalize to the experimental measurements. Although this strategy may work when the true propagation model can be approximated with sufficient accuracy, it is infeasible in wind-tunnel environments because of the complex acoustic phenomena involved, such as vortex shedding at the airfoil trailing edge and nozzle lips, or leading-edge noise caused by inflow turbulence.

Consequently, training should be performed using only the measurements, and the unfolded solver should be adaptive not only to different sensing matrices but also to variations in the regularization strength. In order to meet these requirements, Sec. 4.1 introduces a FISTA-based unfolded algorithm that is trained in an unsupervised way by relying on past model selections with FISTA.

4.1 Unsupervised Ada-NA-LFISTA

Starting from the FISTA extrapolation in Eqs. (6) and (7), one unfolded iteration can be written as

$$x^{(k+1)} = S^{+}_{\theta^{(k)}}\left(z^{(k)} + \gamma^{(k)}\Phi\left(y - Az^{(k)}\right)\right), \tag{10}$$

where $\theta^{(k)}$ and $\gamma^{(k)}$ denote iteration-dependent threshold and step-size parameters at iteration k. Many of the past studies on unfolded ISTA variants have focused on finding suitable representations of Φ to accelerate convergence and to improve reconstruction quality. Classical Learned Iterative Shrinkage-Thresholding Algorithm (LISTA)-type approaches [15] treat Φ as a learnable weight matrix. By contrast, some data-independent variants determine the corresponding operator offline. Analytic Learned ISTA (ALISTA) [24] uses a coherence-minimization approach, whereas Trainable ISTA (TISTA) [18] uses the regularized inverse for ill-conditioned problems and the Moore-Penrose pseudoinverse otherwise instead of $A^{\top}$. However, all of these approaches were derived for a fixed sensing matrix. To accommodate varying sensing matrices, the adaptive formulation of Adaptive Learned FISTA (Ada-LFISTA) is adopted:

$$\Phi = A^{\top}W^{\top}, \tag{11}$$

with a trainable matrix $W \in \mathbb{R}^{m\times m}$. It was shown in [1, Theorem 2] and experiments that Ada-LFISTA yields stable convergence for varying sensing matrices and under model mismatch.

As shown in Fig. 3(b), the selected regularization parameters vary substantially across measurements. Given the connection between the choice of the threshold and the regularization strength, a single set of fixed layer-wise thresholds and step sizes is therefore unlikely to be optimal for the entire dataset. Following the idea of Neural-Augmented ALISTA (NA-ALISTA), these parameters are instead predicted from the current reconstruction state. The state vector is defined as

$$s^{(k)} = \begin{bmatrix} r^{(k)} \\ u^{(k)} \end{bmatrix} = \begin{bmatrix} \|Ax^{(k)} - y\|_1 \\ \|\Phi(Ax^{(k)} - y)\|_1 \end{bmatrix} \in \mathbb{R}^2. \tag{12}$$

Here, $r^{(k)}$ gives the current data mismatch and $u^{(k)}$ serves as a measure of the unknown reconstruction error. These two quantities are passed to an Long Short-Term Memory (LSTM) network. The initial cell state and hidden state are given by

$$q^{(0)} = q_0 \in \mathbb{R}^{d_H}, \qquad h^{(0)} = h_0 \in \mathbb{R}^{d_H}, \tag{13}$$

and the adaptive parameters are predicted as

$$\left(q^{(k)}, h^{(k)}\right) = \mathrm{LSTM}\left(s^{(k)}, q^{(k-1)}, h^{(k-1)}\right), \qquad k = 1, \ldots, K, \tag{14}$$

$$\begin{bmatrix} \theta^{(k)} \\ \gamma^{(k)} \end{bmatrix} = \mathrm{Softsign}\left(Bq^{(k)}\right), \qquad B \in \mathbb{R}^{2\times d_H}. \tag{15}$$

For all experiments in this work, $d_H = 128$.

4.2 Training

Only a few publications have investigated unsupervised training of unfolded algorithms by directly minimizing the objective of the underlying optimization problem, namely the Lasso objective defined in Eq. (4) [2, 27]. A drawback of this training strategy is that the regularization parameter λ must be provided. Given the structural similarity between model-based FISTA and its unfolded variants, previously determined regularization parameters from the model-based optimization provide a natural choice. Following this idea, Ada-NA-LFISTA is trained with the weighted per-sample Lasso loss

$$\mathscr{L}_d = \sum_{k=1}^{K} w^{K-k} \Big(\frac{1}{2} \left\| A\hat{x}^{(k)} - \hat{y} \right\|_2^2 + \hat{\lambda} \, \|\hat{x}^{(k)}\|_1 \Big). \tag{16}$$

For readability, the sample index d is omitted from A, $\hat{y}$, $\hat{\lambda}$, and $\hat{x}^{(k)}$ in Eq. (16). The training objective is obtained by averaging $\mathscr{L}_d$ over batches of sample problems drawn from the dataset $\mathscr{D} = \{(A^{(d)}, \hat{y}^{(d)}, \hat{\lambda}^{(d)})\}_{d=1}^{D}$. This dataset consists of the post-processed measurements described in Sec. 3. Measurements with a flow speed of $U \leq 25\,\mathrm{m/s}$ were excluded. The remaining data were split into training, validation, and test sets containing 80%, 10%, and 10% of the measurements, respectively. As in [11], weighted losses from intermediate iterations were included in the overall loss with $w = 0.5$. In the present experiments, this improved training convergence and stability compared with using only the final iterate. The measurement vector was normalized by the trace of the measured CSM, i.e., $\hat{y} = y/\mathrm{Tr}(C)$. Accordingly, $\hat{\lambda} = \lambda/\mathrm{Tr}(C)$ and $\hat{x} = x/\mathrm{Tr}(C)$.

End-to-end training of the model was performed on a NVIDIA GeForce RTX 3090 using the Adam optimization algorithm with an initial learning rate of 5×10^{-4} and a batch size of 64 reconstruction problems. The loss was evaluated on the validation set every 500 training iterations. If the validation loss did not improve for 10 consecutive evaluations, the learning rate was reduced by a factor of 0.5. Training was stopped once the learning rate reached 5×10^{-6}, and the model with the lowest validation loss was selected.

5 RESULTS

5.1 Convergence Behavior

The convergence behavior of the CMF method with Ada-NA-LFISTA is compared with that of model-based FISTA on the test dataset over the first $K = 50$ iterations. Figures 4 and 5 show the median normalized BIC, the median relative residual error

$$\varepsilon_\mathrm{r} = \frac{\|Ax - y\|_2^2}{\|y\|_2^2}, \tag{17}$$

and the median sparsity, quantified by the number of non-zero entries $\|x\|_0$, of the reconstructed source maps as functions of the iteration count. The gray areas indicate iterations beyond the training depth of the unfolded model, namely $K = 10$ at 8 kHz and $K = 30$ at 4 kHz.

At 8 kHz, training Ada-NA-LFISTA beyond $K = 10$ did not lead to further improvements at later iterates. Nevertheless, when the trained model is evaluated up to $K = 50$, it remains stable

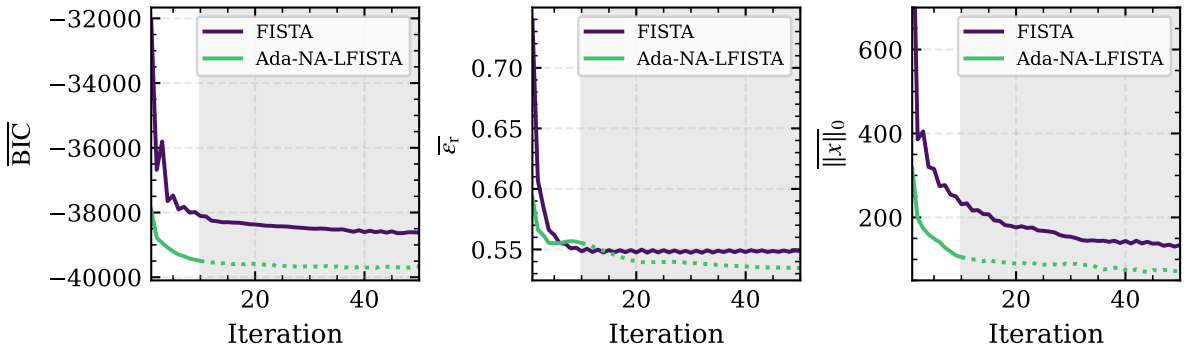

Figure 4: Median convergence curves of Ada-NA-LFISTA and FISTA over the test dataset at 8 kHz. *The plots show the median normalized BIC, the median relative residual error* ε_r*, and the median sparsity* $\|x\|_0$ *as functions of the iteration number. The gray area marks iterations beyond the training depth of the unfolded model, i.e.,* $K > 10$.

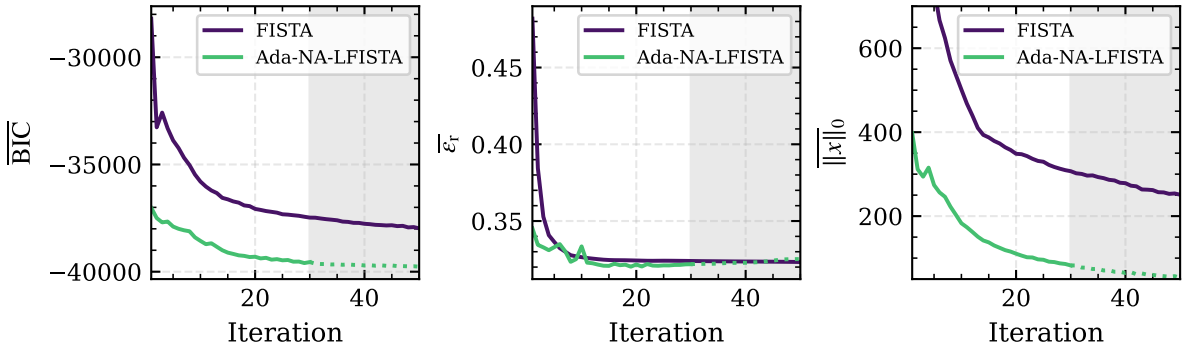

Figure 5: Median convergence curves of Ada-NA-LFISTA and FISTA over the test dataset at 4 kHz. *The plots show the median normalized BIC, the median relative residual error* ε_r*, and the median sparsity* $\|x\|_0$ *as functions of the iteration number. The gray area marks iterations beyond the training depth of the unfolded model, i.e.,* $K > 30$.

and consistently outperforms FISTA over the entire range, exhibiting a lower BIC, a lower relative residual error, and sparser reconstructed source maps. In addition, ε_r continues to decrease slightly beyond the training depth, which indicates limited but favorable generalization beyond the training depth. A similar effect was observed for NA-ALISTA in [21].

At 4 kHz, stable behavior up to $K = 50$ required training with at least $K = 30$ unfolded iterations. In this case, Ada-NA-LFISTA again achieves a substantially lower BIC and much sparser reconstructions than FISTA throughout the first 50 iterations. The residual error, however, is only slightly lower at early iterations and becomes slightly higher than that of FISTA at later iterations, indicating potential overfitting to the training depth. Overall, the behavior of Ada-NA-LFISTA beyond the training depth appears stable over a limited range of iterations, but it is frequency-dependent and cannot be assumed a priori.

Table 2 summarizes the median values of BIC, ε_r, and $\|x\|_0$ for Ada-NA-LFISTA at $K = 50$

Table 2: Median values of the evaluation metrics BIC, ε_r, and $\|x\|_0$ over the test dataset for Ada-NA-LFISTA at $K = 50$ and FISTA at $K = 10{,}000$, shown for 8 kHz and 4 kHz.

	8 kHz			4 kHz		
Method	$\overline{\text{BIC}}$	$\overline{\varepsilon_r}$	$\overline{\|x\|_0}$	$\overline{\text{BIC}}$	$\overline{\varepsilon_r}$	$\overline{\|x\|_0}$
Ada-NA-LFISTA (K=50)	-39671	0.535	75	-39766	0.325	53
FISTA (K=10000)	-38681	0.549	112	-39816	0.320	48

and FISTA at $K = 10{,}000$. At 8 kHz, Ada-NA-LFISTA outperforms the model-based FISTA in all three metrics despite using 200 times fewer iterations. At 4 kHz, the Ada-NA-LFISTA achieves a similar performance with slightly higher ε_r, BIC, and slightly lower sparsity compared to FISTA with 10,000 iterations.

5.2 Source Mappings

A qualitative comparison of the reconstructed source maps is shown in Figs. 6 and 7 for 8 kHz and 4 kHz, respectively. In addition to Ada-NA-LFISTA and FISTA, the comparison includes orthogonal deconvolution [31], CLEAN Based on Spatial Source Coherence (CLEAN-SC) [37], DAMAS [6], and CMF solved by tuning-free NNLS, all implemented in Acoular [34]. For CLEAN-SC, a damping factor of 0.6 was used. The source maps are shown for the tripped baseline airfoil at a geometric angle of attack of 0.8° and flow speeds of 49.5 m s^{-1} and 35.3 m s^{-1} at 8 kHz and 4 kHz, respectively. The source contributions inside the rectangular sector associated with trailing-edge noise were integrated; the resulting levels are given in the lower-right corner of each source map. The remaining corners show the per-sample values of ε_r, BIC, and $\|x\|_0$.

At both frequencies, the dominant reconstructed sources are concentrated at the trailing edge. Among the compared methods, Ada-NA-LFISTA provides a favorable trade-off between sparsity and agreement with the measurements. Its reconstructions remain focused on physically plausible source regions and are markedly sparser than those of CMF with NNLS, while still achieving competitive values of ε_r and BIC. At 8 kHz, Ada-NA-LFISTA yields one of the lowest BIC values among all methods while maintaining a sparse reconstruction. At 4 kHz, it remains competitive with FISTA, DAMAS, and CLEAN-SC. By contrast, CMF with NNLS attains the closest agreement with the measurements, as indicated by the lowest residual error at both frequencies, but this comes at the cost of many additional source contributions in regions where no physical sources are expected. The trailing-edge sector integration confirms that Ada-NA-LFISTA yields meaningful source-strength estimates. At 8 kHz, the integrated level obtained with Ada-NA-LFISTA is close to the values obtained with FISTA, DAMAS, and CLEAN-SC, with a maximum deviation of 0.9 dB. At 4 kHz, the agreement is even closer, with a maximum deviation of 0.7 dB relative to these methods.

5.3 Computational Efficiency

Table 3 compares the processing time for a single measurement at 8 kHz. The comparison starts after the CSM has been estimated and after the propagation model has been computed. These preprocessing steps are therefore excluded for all methods. The timing of FISTA includes model

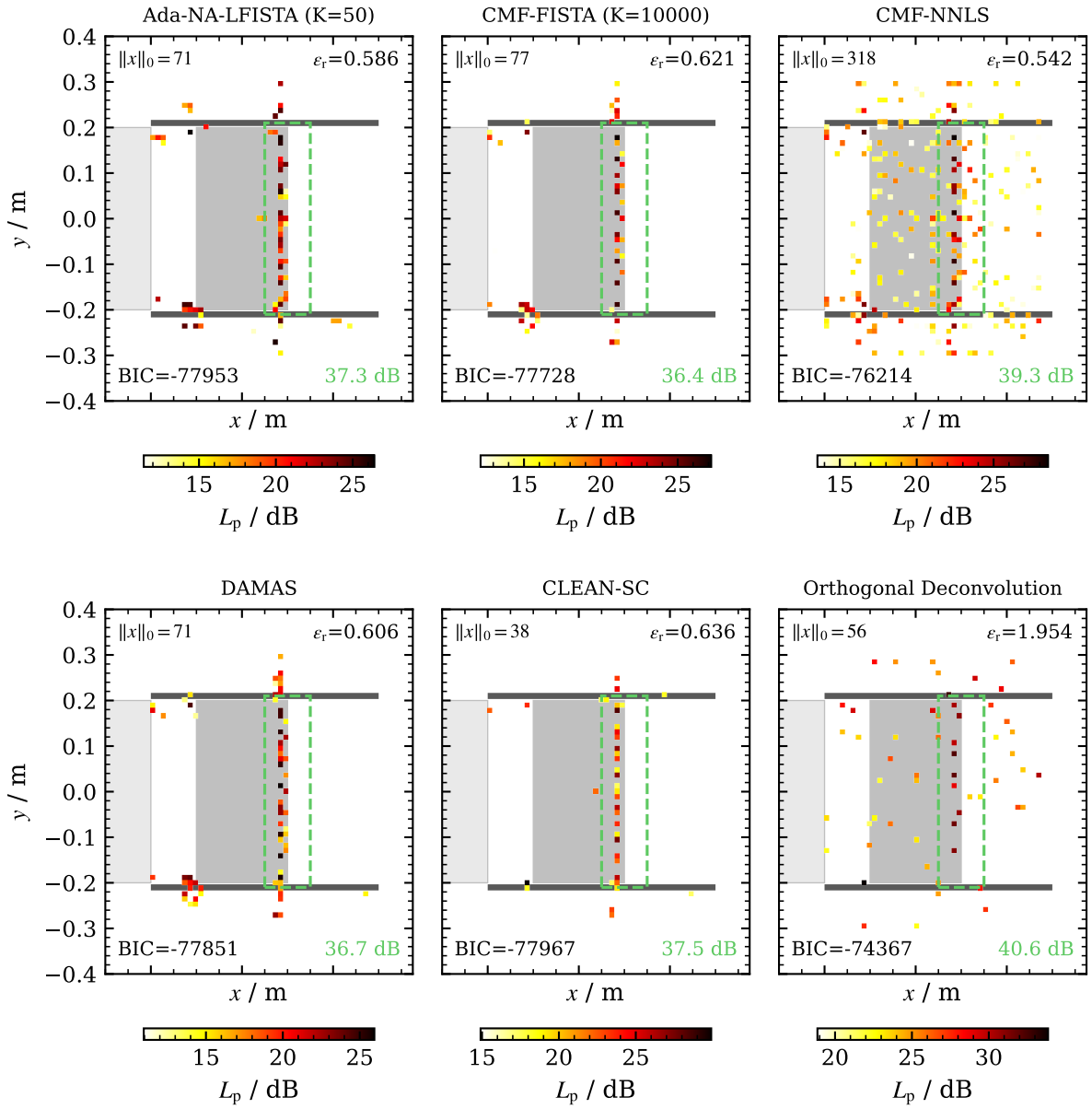

Figure 6: Source map reconstructions at 8 kHz *with Ada-NA-LFISTA, FISTA, orthogonal deconvolution, CLEAN-SC, DAMAS, and CMF with NNLS (geometric angle of attack* 0.8°*,* $U = 49.5\,\mathrm{m\,s^{-1}}$*, baseline, tripped).*

selection by grid search over the regularization parameter. The grid search was evaluated on the GPU and parallelized across the regularization grid. The training and evaluation of Ada-NA-LFISTA were also performed on the GPU. Training took several hours on a single NVIDIA GeForce RTX 3090 GPU. After training, Ada-NA-LFISTA does not require a separate model-selection step. The learned update rules depend on the data and impose sparsity implicitly through the unfolded iterations. For the example in Table 3, this results in an average processing

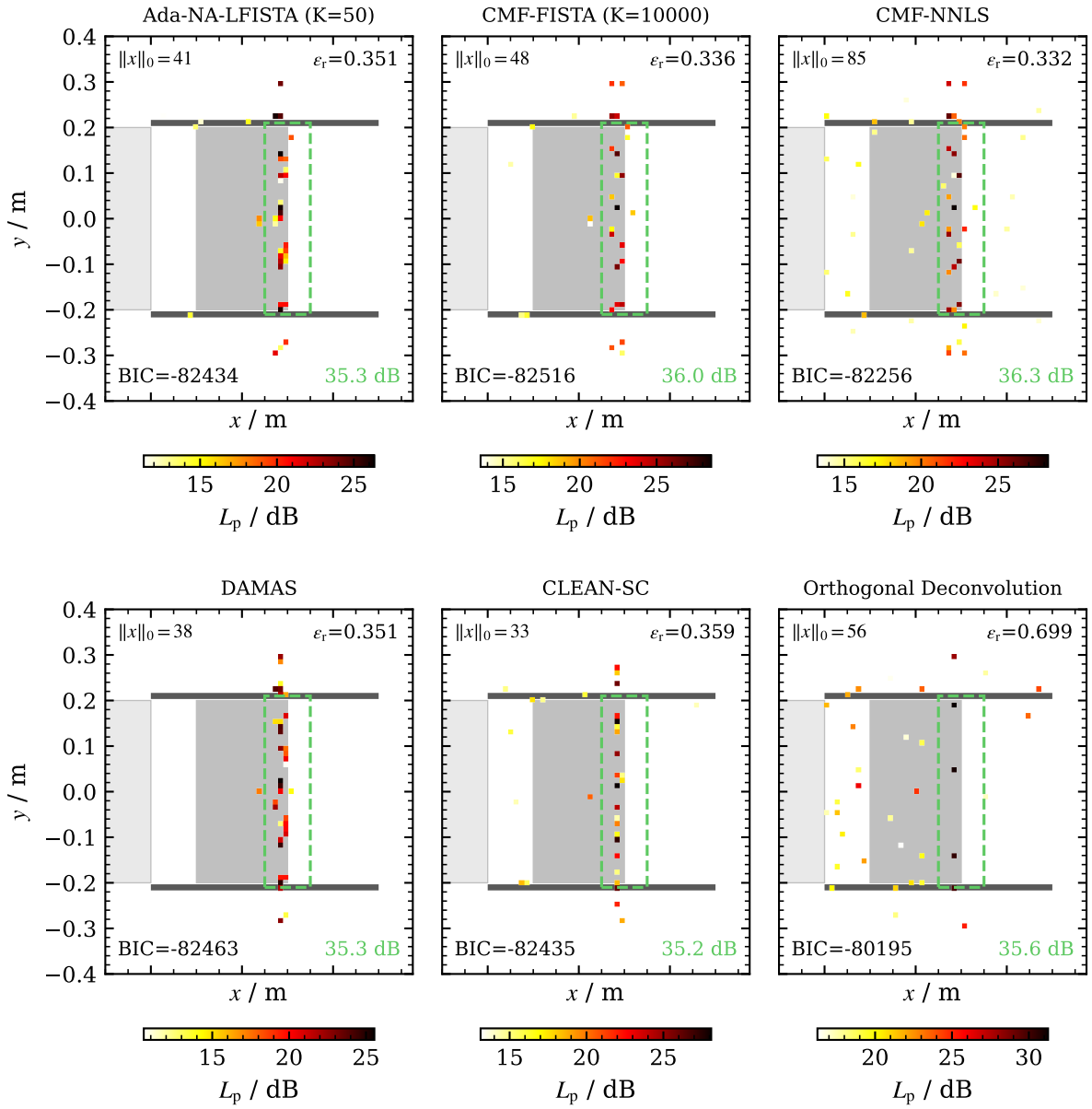

Figure 7: Source map reconstructions at 4 kHz *with Ada-NA-LFISTA, FISTA, orthogonal deconvolution, CLEAN-SC, DAMAS, and CMF with NNLS (geometric angle of attack* 0.8°*,* $U = 35.3\,\mathrm{m\,s^{-1}}$*, baseline, tripped).*

time of 0.33 s per measurement. This is considerably faster than FISTA with model selection, CMF with NNLS, and DAMAS. It is slower than CLEAN-SC and orthogonal deconvolution, but remains within the same order of magnitude as these fast deconvolution methods.

The simple iterative structure of Ada-NA-LFISTA also allows parallel evaluation across multiple measurements. This is useful for larger measurement sets, where many source maps have to be computed for the same frequency.

Table 3: Mean and standard deviation of the processing time per measurement at 8 kHz*. The calculation time for the* CSM *and ray-casting is not included.*

Method	Mean time / s	Std. / s
Ada-NA-LFISTA (K=50)	0.33	0.05
CMF-FISTA (K=10,000)	8.64	0.79
CMF-NNLS	6.37	0.32
DAMAS	2.66	0.19
CLEAN-SC	0.05	0.02
Orthogonal Deconvolution	0.13	0.01

6 CONCLUSIONS

This contribution has shown that unfolded proximal-gradient algorithms can be trained directly on measured aeroacoustic microphone array data by minimizing the Lasso objective, without requiring ground-truth source maps. For the investigated airfoil dataset, the proposed Ada-NA-LFISTA has yielded plausible source mappings and a favorable trade-off between sparsity and agreement with the measured data. Across both analyzed frequencies, it produced reconstruction results similar to those of model-based FISTA while requiring far fewer iterations. In this sense, deep unfolding has provided not only acceleration, but also a practical way of learning implicit regularization from past model selections. The main practical implication is that source reconstruction can be performed without a separate model-selection step once training has been completed. For the present setup, this reduced the mean runtime at 8 kHz from 8.64 s for FISTA with model selection to 0.33 s per measurement. Still, the training effort remains substantial because separate models were trained per frequency. Future work should therefore focus on reducing training costs, for example by exploring transfer-learning strategies.

ACKNOWLEDGEMENTS

The authors thank Gert Herold and Roxanna Donner for performing the microphone array measurements that provided the data used in this work. The authors also thank Arya Prasetya for help in developing the underlying source code.

References

[1] A. Aberdam, A. Golts, and M. Elad. "Ada-LISTA: Learned Solvers Adaptive to Varying Models." *IEEE Transactions on Pattern Analysis and Machine Intelligence*, 44(12), 9222–9235, 2022. doi:10.1109/TPAMI.2021.3125041.

[2] P. Ablin, T. Moreau, M. Massias, and A. Gramfort. "Learning step sizes for unfolded sparse coding." In *Advances in Neural Information Processing Systems*, volume 32. 2019.

[3] R. Balaji, K.-L. Chen, and B. D. Rao. "A Structured Neural Network Approach for Learning Improved Iterative Algorithms for SBL." In *2025 IEEE International Conference*

on Acoustics, Speech, and Signal Processing, pages 1–5. IEEE, Hyderabad, India, 2025. ISBN 979-8-3503-6874-1. doi:10.1109/ICASSP49660.2025.10890518.

[4] A. Beck and M. Teboulle. "A Fast Iterative Shrinkage-Thresholding Algorithm for Linear Inverse Problems." *SIAM Journal on Imaging Sciences*, 2(1), 183–202, 2009. ISSN 1936-4954. doi:10.1137/080716542.

[5] F. Behrens, J. Sauder, and P. Jung. "Neurally Augmented ALISTA." In *International Conference on Learning Representations*. 2021.

[6] T. F. Brooks and W. M. Humphreys. "A deconvolution approach for the mapping of acoustic sources (DAMAS) determined from phased microphone arrays." *Journal of Sound and Vibration*, 294(4), 856–879, 2006. ISSN 10958568. doi:10.1016/j.jsv.2005.12.046.

[7] F. Chen, Y. Xiao, L. Yu, L. Chen, and C. Zhang. "Extending FISTA to FISTA-Net: Adaptive reflection parameters fitting for the deconvolution-based sound source localization in the reverberation environment." *Mechanical Systems and Signal Processing*, 210, 111130, 2024. ISSN 08883270. doi:10.1016/j.ymssp.2024.111130.

[8] T. Chen, X. Chen, W. Chen, Z. Wang, H. Heaton, J. Liu, and W. Yin. "Learning to Optimize: A Primer and A Benchmark." *The Journal of Machine Learning Research*, 23(1), 8562–8620, 2022.

[9] X. Chen, J. Liu, Z. Wang, and W. Yin. "Theoretical Linear Convergence of Unfolded ISTA and Its Practical Weights and Thresholds." In *Advances in Neural Information Processing Systems 31*, pages 9061–9071. 2018.

[10] X. Chen, J. Liu, Z. Wang, and W. Yin. "Hyperparameter tuning is all you need for LISTA." In *Advances in Neural Information Processing Systems*, volume 34. 2021.

[11] Y. Chen, X. Chen, A. Maleki, and S. Jalali. "Comprehensive examination of unrolled networks for solving linear inverse problems." *Entropy*, 27(9), 2025. ISSN 1099-4300. doi:10.3390/e27090929.

[12] A. Dinsenmeyer, J. Antoni, Q. Leclère, and A. Pereira. "A probabilistic approach for cross-spectral matrix denoising: Benchmarking with some recent methods." *The Journal of the Acoustical Society of America*, 147(5), 3108–3123, 2020. ISSN 0001-4966. doi:10.1121/10.0001098.

[13] R. P. Dougherty. "Turbulent decorrelation of aeroacoustic phased arrays: Lessons from atmospheric science and astronomy." In *9th AIAA/CEAS Aeroacoustics Conference and Exhibit*. American Institute of Aeronautics and Astronautics, Hilton Head, South Carolina, 2003. doi:10.2514/6.2003-3200.

[14] A. Fischer, O. Lylloff, C. Bak, A. S. Olsen, F. Bertagnolio, S. Luesutthiviboon, T. L. Pereira, D. Ragni, F. Avallone, D. Cassalino, M. Herr, C. Appel, and J. M. Pereira-Gomes. "Iea task 39: Wind tunnel serration benchmark." Technical report, Technical University of Denmark and Delft University of Technology and German Aerospace Center and DNW, 2021.

[15] K. Gregor and Y. LeCun. "Learning Fast Approximations of Sparse Coding." In *Proceedings of the 27th International Conference on International Conference on Machine Learning*, pages 399–406. Omnipress, Haifa, Israel, 2010. ISBN 978-1-60558-907-7.

[16] J. C. Hauffen, P. Jung, and N. Mücke. "Algorithm unfolding for block-sparse and MMV problems with reduced training overhead." *Frontiers in Applied Mathematics and Statistics*, 9, 1205959, 2023. ISSN 2297-4687. doi:10.3389/fams.2023.1205959.

[17] G. Herold and E. Sarradj. "Performance analysis of microphone array methods." *Journal of Sound and Vibration*, 401, 152–168, 2017. ISSN 10958568. doi:10.1016/j.jsv.2017.04.030.

[18] D. Ito, S. Takabe, and T. Wadayama. "Trainable ISTA for Sparse Signal Recovery." *IEEE Transactions on Signal Processing*, 67(12), 3113–3125, 2019. ISSN 19410476. doi:10.1109/TSP.2019.2912879.

[19] C. Kayser, A. Kujawski, and E. Sarradj. "A fast data-driven method for inverse microphone array signal processing." *JASA Express Letters*, 3(4), 042401, 2023. ISSN 2691-1191. doi:10.1121/10.0017882.

[20] D. Kim and D. Park. "Element-Wise Adaptive Thresholds for Learned Iterative Shrinkage Thresholding Algorithms." *IEEE Access*, 8, 45874–45886, 2020. ISSN 2169-3536. doi:10.1109/ACCESS.2020.2978237.

[21] A. Kujawski and E. Sarradj. "Parameter-efficient unfolded networks for inverse microphone array processing." In *Fortschritte der Akustik - DAGA 2026, 52. Jahrestagung für Akustik*, pages 156–159. Deutsche Gesellschaft für Akustik e.V. (DEGA), Dresden, 2026. ISBN 978-3-939296-24-9. doi:10.71568/daga2026.493.

[22] Z. Li, K. Wu, Y. Guo, and C. Zhang. "Learned ISTA with Error-Based Thresholding for Adaptive Sparse Coding." In *2024 IEEE International Conference on Acoustics, Speech, and Signal Processing*. IEEE, Seoul, Korea, Republic of, 2024. doi:10.1109/ICASSP48485.2024.10446361.

[23] W. Liang, J. Liu, and J. Zhu. "Improved Analytic Learned Iterative Shrinkage Thresholding Algorithm and Its Application to Tomographic Synthetic Aperture Radar Building Object Height Inversion." *Mathematics*, 12(10), 1464, 2024. ISSN 2227-7390. doi:10.3390/math12101464.

[24] J. Liu, X. Chen, Z. Wang, and W. Yin. "ALISTA: ANALYTIC WEIGHTS ARE AS GOOD AS LEARNED WEIGHTS IN LISTA." In *International Conference on Learning Representations*. 2019.

[25] R. Merino-Martínez, P. Sijtsma, M. Snellen, T. Ahlefeldt, J. Antoni, C. J. Bahr, D. Blacodon, D. Ernst, A. Finez, S. Funke, T. F. Geyer, S. Haxter, G. Herold, X. Huang, W. M. Humphreys, Q. Leclère, A. Malgoezar, U. Michel, T. Padois, A. Pereira, C. Picard, E. Sarradj, H. Siller, D. G. Simons, and C. Spehr. *A review of acoustic imaging methods using phased microphone arrays*, volume 10. Springer Vienna, 2019. ISBN

0-12-345678-9. doi:10.1007/s13272-019-00383-4. URL http://link.springer.com/10.1007/s13272-019-00383-4.

[26] V. Monga, Y. Li, and Y. C. Eldar. "Algorithm Unrolling: Interpretable, Efficient Deep Learning for Signal and Image Processing." *IEEE Signal Processing Magazine*, 38(2), 18–44, 2021. ISSN 1053-5888, 1558-0792. doi:10.1109/MSP.2020.3016905.

[27] K. Nagahisa, R. Hayakawa, and Y. Iiguni. "Comparison between Supervised and Unsupervised Learning in Deep Unfolded Sparse Signal Recovery.", 2025. doi:10.48550/arXiv.2509.01331. URL http://arxiv.org/abs/2509.01331.

[28] R. Pagoti, S. Tenneti, R. Ramu Naidu, and P. Sasmal. "Learned-Map-Omp: An Unrolled Neural Network for Signal and Image Denoising.", 2024. doi:10.2139/ssrn.5062651. URL https://www.ssrn.com/abstract=5062651.

[29] W. Pu, C. Zhou, Y. C. Eldar, and M. R. D. Rodrigues. "REST: Robust lEarned Shrinkage-Thresholding Network Taming Inverse Problems with Model Mismatch." In *2021 IEEE International Conference on Acoustics, Speech, and Signal Processing*, pages 2885–2889. IEEE, Toronto, ON, Canada, 2021. ISBN 978-1-7281-7605-5. doi:10.1109/ICASSP39728.2021.9414141.

[30] H.-G. Raumer, D. Ernst, and C. Spehr. "Compensation of Modeling Errors for the Aeroacoustic Inverse Problem with Tools from Deep Learning." *Acoustics*, 4(4), 834–848, 2022. doi:10.3390/acoustics4040050.

[31] E. Sarradj. "A fast signal subspace approach for the determination of absolute levels from phased microphone array measurements." *Journal of Sound and Vibration*, 329(9), 1553–1569, 2010. ISSN 0022460X. doi:10.1016/j.jsv.2009.11.009.

[32] E. Sarradj. "A Generic Approach To Synthesize Optimal Array Microphone Arrangements." In *Proceedings of the 6th Berlin Beamforming Conference*, pages 1–12. February 29 – March 1, Berlin, Germany, 2016. ISBN 978-3-942709-15-6.

[33] E. Sarradj. "A fast ray casting method for sound refraction at shear layers." *International Journal of Aeroacoustics*, 16(1-2), 65–77, 2017. doi:10.1177/1475472X16680463.

[34] E. Sarradj and G. Herold. "A Python framework for microphone array data processing." *Applied Acoustics*, 116, 50–58, 2017. ISSN 1872910X. doi:10.1016/j.apacoust.2016.09.015.

[35] A. Sen, P. Pradhan, R. Randhi, and C. S. Sastry. "Unrolled Proximal Gradient Descent Method for Non-Negative Least Squares Problem." In *2024 IEEE International Conference on Acoustics, Speech, and Signal Processing*, pages 7625–7629. IEEE, Seoul, Korea, Republic of, 2024. ISBN 979-8-3503-4485-1. doi:10.1109/ICASSP48485.2024.10447946.

[36] P. Sijtsma. "Experimental techniques for identification and characterisation of noise sources." Technical Report NLR-TP-2004-165, National Aerospace Laboratory NLR, 2004. URL https://reports.nlr.nl/server/api/core/bitstreams/9108ade9-4d4a-4d4a-a979-ddec2ff3079f/content.

[37] P. Sijtsma. "CLEAN Based on Spatial Source Coherence." *International Journal of Aeroacoustics*, 6(4), 357–374, 2007. ISSN 1475-472X. doi:10.1260/147547207783359459.

[38] P. Sijtsma, R. Merino-Martinez, A. M. N. Malgoezar, and M. Snellen. "High-resolution CLEAN-SC: Theory and experimental validation." *International Journal of Aeroacoustics*, 16(4-5), 274–298, 2017. ISSN 20484003. doi:10.1177/1475472X17713034.

[39] R. Tibshirani, J. Bien, J. Friedman, T. Hastie, N. Simon, J. Taylor, and R. J. Tibshirani. "Strong Rules for Discarding Predictors in Lasso-Type Problems." *Journal of the Royal Statistical Society Series B: Statistical Methodology*, 74(2), 245–266, 2012. ISSN 1369-7412, 1467-9868. doi:10.1111/j.1467-9868.2011.01004.x.

[40] H. Vogel. "A better way to construct the sunflower head." *Mathematical Biosciences*, 44(3), 179–189, 1979. ISSN 0025-5564. doi:10.1016/0025-5564(79)90080-4.

[41] P. D. Welch. "The use of fast Fourier transform for the estimation of power spectra: A method based on time averaging over short, modified periodograms." *IEEE Transactions on Audio and Electroacoustics*, 15(2), 70–73, 1967. doi:10.1109/TAU.1967.1161901.

[42] Y. Wu and L. Wang. "A Survey of Tuning Parameter Selection for High-Dimensional Regression." *Annual Review of Statistics and Its Application*, 7, 209–226, 2020. doi:10.1146/annurev-statistics-030718-105038.

[43] J. Xiang, Y. Dong, and Y. Yang. "FISTA-Net: Learning A Fast Iterative Shrinkage Thresholding Network for Inverse Problems in Imaging." *IEEE Transactions on Medical Imaging*, 40(5), 1329–1339, 2021. ISSN 0278-0062, 1558-254X. doi:10.1109/TMI.2021.3054167.

[44] J. Xiang, Y. Dong, and Y. Yang. "FISTA-Net: Learning A Fast Iterative Shrinkage Thresholding Network for Inverse Problems in Imaging." *IEEE Transactions on Medical Imaging*, 40(5), 1329–1339, 2021. ISSN 0278-0062, 1558-254X. doi:10.1109/TMI.2021.3054167.

[45] T. Yardibi, J. Li, P. Stoica, and L. N. Cattafesta. "Sparsity constrained deconvolution approaches for acoustic source mapping." *The Journal of the Acoustical Society of America*, 123(5), 2631–2642, 2008. doi:http://dx.doi.org/10.1121/1.2896754.

[46] T. Yardibi, J. Li, P. Stoica, N. S. Zawodny, and L. N. Cattafesta. "A covariance fitting approach for correlated acoustic source mapping." *The Journal of the Acoustical Society of America*, 127(5), 2920–2931, 2010. ISSN 0001-4966. doi:10.1121/1.3365260.

[47] J. Zhang and B. Ghanem. "ISTA-Net: Interpretable Optimization-Inspired Deep Network for Image Compressive Sensing." In *2018 IEEE/CVF Conference on Computer Vision and Pattern Recognition*, pages 1828–1837. IEEE, Salt Lake City, UT, 2018. ISBN 978-1-5386-6420-9. doi:10.1109/CVPR.2018.00196.

[48] L. Zhang, Y. Hu, C. K. W. Yu, and J. Wang. "Iterative positive thresholding algorithm for non-negative sparse optimization." *Optimization*, 67(9), 1345–1363, 2018. ISSN 0233-1934, 1029-4945. doi:10.1080/02331934.2018.1470629.